# Water-soluble bio-sourced resist interactions with fluorinated etching plasmas during the photolithography process

Paule Durin, Olha Sysova, Alexandre Téolis, Stéphane Trombotto, Samar Hajjar-Garreau, Thierry Delair, Isabelle Servin, Névine Rochat, Raluca Tiron, Corinne Gablin, et al.

# Water-soluble bio-sourced resist interactions with fluorinated etching plasmas during the photolithography process

Paule Durin[1,2], Olha Sysova[3,4], Alexandre Téolis[5,6], Stéphane Trombotto[5], Samar Hajjar-Garreau[3, 4], Thierry Delair[5], Isabelle Servin[6], Névine Rochat[6], Raluca Tiron[6], Corinne Gablin[2], Olivier Soppera[3,4], Aziz Benamrouche[1], Thomas Géhin[1], Didier Léonard[2 a)], Jean-Louis Leclercq[1 a)], Yann Chevolot[1,a)]

[1] Univ Lyon, CNRS, INSA Lyon, Ecole Centrale de Lyon, Université Claude Bernard Lyon 1, CPE Lyon, INL, UMR5270, 69130 Ecully, France
[2] Univ Lyon, CNRS, Université Claude Bernard Lyon 1, Institut des Sciences Analytiques, UMR 5280, 69100 Villeurbanne, France
[3] Université de Haute-Alsace, CNRS, IS2M, UMR 7361, 68100 Mulhouse, France
[4] Université de Strasbourg, France
[5] Univ Lyon, CNRS, UMR 5223, Ingénierie des Matériaux Polymères, Université Claude Bernard Lyon 1, INSA Lyon, Université Jean Monnet, F-69622 Villeurbanne Cedex, France
[6] Univ. Grenoble Alpes, CEA, LETI, F-38000 Grenoble, France

[a)] Electronic mail: yann.chevolot@ec-lyon.fr, Jean-Louis.Leclercq@ec-lyon.fr, didier.leonard@univ-lyon1.fr

## Abstract:

Lithography is one of the key steps in micro/nanofabrication which involves the use of oil-based resists, organic solvents and toxic chemicals. Nowadays, environmental issues and regulation have raised the need for developing greener materials and processes. Therefore, efforts have been devoted in developing greener resists, in particular resists based on water-soluble bio-sourced polymers. Among these biopolymers, polysaccharides have gained a strong interest. However, their interaction with silica etching plasmas, in particular fluorinated plasmas, remains scarcely studied and contradictory results are found in the literature. The present contribution reports on the study of the interaction of two chitosans exhibiting different degrees of *N*-acetylation (DA) with $SF_6$/Ar and $CHF_3$ etching plasmas. The surface modifications and in-depth modifications were studied with X-ray Photoelectron Spectroscopy (XPS), Time-of-Flight Secondary Ion Mass Spectrometry

(ToF-SIMS), Infra-red spectroscopy (IR), water contact angle and size exclusion chromatography (SEC). The effect of neutrals, ions and Vacum ultraviolet (VUV) was considered. Our results suggest that the chitosan selectivity is greatly influenced by the deposition of a fluorocarbon film and that VUV seems to be involved in scissions of the polymer chains. No significant difference between the two chitosans was observed.

# I. INTRODUCTION

High density Integrated Circuit (IC) device fabrication requires manufacturing methods that possess micrometer to nanometer-scale resolution. This ability to downscale the critical dimensions of IC devices has been achievable thanks to the improvement in the microlithography techniques and materials used to produce the patterned layers of single IC devices. Microlithography techniques refer to the processes involving pattern-transfer of the desired micro- or nano-scale features from an IC design into the semiconductor device. It involves a variety of steps ranging from mask realization to the development of high-fidelity patterns in a photoresist film followed either by an etching step or by a deposition step. Etching can be performed using wet chemistry, but dry etching by plasma (e.g. fluorinated plasmas to etch silica) offers several key advantages, in particular its anisotropic character[1].

Nowadays with the global warming issue and the quest for greener and less toxic manufacturing processes, health and environmental concerns have been raised for the lithography process. In fact, the chemicals used to produce the resin, the additives, the chemical synthesis, the solvents and the developers are all issued from petroleum and among them, some are dangerous and toxic[2,3] (i.e. Tetramethylammonium hydroxide, TMAH). In order to develop a more sustainable technology, several authors have proposed to replace these conventional petroleum-based resists by water soluble bio-sourced polymers. Bio-sourced resists reported in the literature are either of protein or polysaccharide nature.

Among others, ovalbumin[4], silk[5–12], and keratin[13] have been proposed as possible protein based resists. Using dry etching ($SF_6/C_4H_8$) and ovalbumin, features were obtained by photolithography at 254 nm and transferred into silicon with an aspect ratio of 1/1[4]. One of the limitations of ovalbumin is the tedious stripping step (15h) and the fact that it is in competition with human food resources. In the case of keratin and silk, both unmodified and acrylate modified proteins were used as resists. $CF_4$ induced coupled plasma was applied to etch silicon[14]. The main influencing parameters[14] on the performance during the etching transfer of a silk film used as a temporary masking layer were the molecular weight, the extent of the cross-linking reaction and the presence of a secondary structure (beta sheets).

In the case of polysaccharide resists, transfer of nanometer scale patterns in silicon using ICP-RIE was achieved with a hemicellulose resist[15]. Aspect ratio of almost 7 was achieved thanks to its 3.7 selectivity. Opposite results were obtained from the group of Takei[16], where a poor selectivity was observed when using glucose or glucans as resist layers in $CF_4$ plasma. A trilayer process was therefore proposed[16]. Furthermore, it was found that Ar plasmas can lead to either cross-linking[17] or chain scissions[18]. Other authors reported that $SF_6$ plasma leads to fluorine incorporation into the chemical structure and cross-linking[19,20]. These results highlight that the mechanism of fluorinated etching plasma interaction with polysaccharides remains to be further investigated.

Several groups have reported the use of chitosan as a resist[21–24]. Chitosan is a linear polysaccharide composed of D-Glucosamine (GlcN) and *N*-acetyl D-glucosamine (GlcNAc). It is characterized by its degree of *N*-acetylation (DA) corresponding to the molar ratio of GlcNAc units within the polymer chain and by its molecular weight.

Chitosan is issued from chitin, which is the second most abundant biopolymer on earth. It is water soluble, water developable and has demonstrated to be a good candidate for E-beam lithography[25] and DUV photolithography[26,27] allowing for the writing of sub-micron features. Contrary to Takei's group, we have been able to transfer the features into a 200 nm silica layer using $CHF_3$ RIE without the need of an additional hard mask. The molecular structures of the polysaccharides used by Takei resists are quite similar to the structure of chitosan, raising the need of a better understanding of the interaction of polysaccharides with fluorinated etching plasmas.

The aim of the present contribution is to gain qualitative insights on the interactions between chitosan and fluorinated plasmas used to etch silica. For this, modifications of 100 nm spin-casted chitosan films submitted to our $CHF_3$ and $SF_6$/Ar standard etching plasma recipes were studied using complementary analytical techniques (IR, XPS, ToF-SIMS, SEC…). Two chitosan resists with DA of 1 and 35 % were compared. The interactions with plasma neutrals/ions and vacuum ultraviolet (VUV) were studied. Our results suggest that the chitosan selectivity is greatly influenced by the deposition of a fluorocarbon film and that VUV seem to be involved in scission of the polymer chain. No significant difference between the two chitosans was observed.

# II. EXPERIMENTAL

## *A. Description of materials*

### *1. Chemicals and resist material*

Chemicals were purchased from Sigma Aldrich except when stated otherwise. Deionized water (18.2 MΩ.cm) was produced with a purelab Chorus (ELGA). Chitosan from squid pens, with a DA of 2 % acetylation degree, an average molecular weight of $M_w$=573 kg.mol$^{-1}$ and a dispersity of 1.59, was purchased from Mahtani Chitosan PVT, Ltd (India). The reacetylation of the chitosan was performed according to the Lamarque's protocol[28]. Briefly, chitosan was first solubilized in a dilute aqueous solution of acetic acid and stirred overnight. Propane-1-2-diol was added and the solution was cooled to approximately 10 °C. Acetic anhydride was added dropwise in stoichiometric quantities based on GlcN units to reach the desired DA. At the end of the reaction, the reacetylated chitosan was fully precipitated by addition of dilute aqueous ammonia to reach pH 9-10, washed several times with deionized water and then freeze-dried. Reacetylated chitosan was obtained with a DA of 35 %, a $M_w$ of 613 kg.mol$^{-1}$ (dispersity of 1.75) and a water content of 13.5 % (w/w). The DA was determined by $^1$H-NMR using a Bruker AV300 (300 MHz) spectrometer.

The average molar masses ($M_w$ and $M_n$) and the dispersity Đ of the chitosan were determined by size exclusion chromatography (SEC). The polymer separation was performed on two serially connected columns (TSK G2500PW and TSK G6000PW, TOSOH BIOSCIENCE). A differential refractometer (Optilab T-rex, WYATT) coupled

on-line with a MALLS detector (Dawn Heleos II, WYATT) was used for the detection. A degassed 0.2 M acetic acid/0.15 M ammonium acetate buffer (pH 4.5) was used as eluent after filtration on a 0.10 µm pore size membrane (Millipore). The flow rate was maintained at 0.5 mL/min and the amount of sample injected was 50 µL. The refractive index increment (dn/dc) was adjusted for each acetylation degree (DA) according to the results of Schatz et al[29].

For comparison purposes, Chitosan with a DA of 1 %, a MW of 583 $kg.mol^{-1}$ (dispersity of 1.66) and water content of 8.9 % (w/w) was also used, as well as commercial positive resists (AZ5214E (EU) from Merck and 950 PMMA A4 from Kayaku Advanced Materials).

## 2. *Solution and film preparation*

Glassware and substrates were systematically cleaned by piranha etch treatment ($H_2SO_4$ 95.0-98.0 %; hydrogen peroxide $H_2O_2$ 34.5-36.5 %; v/v 3:1) to prevent from organic contamination.

Chitosan solutions were prepared by dissolving chitosan in deionized water and acetic acid in stoichiometric quantity[28] (with respect to GlcN units). Chitosan concentration was 0.7 % (w/v). Solutions were magnetically stirred overnight, at room temperature and in the dark. Characteristics of chitosan based resists used in this article are summarized in TABLE I.

TABLE I. Chitosan based resists used in this study

| Resist name | DA (%) | Concentration % (w/v) | Mw ($kg.mol^{-1}$) | Water content (%) |
|---|---|---|---|---|
| Ch1 | 1 | 0.7 | 583 | 8.9 |
| Ch35 | 35 | 0.7 | 613 | 13.5 |

The majority of the chitosan films were processed as follows. Thick silicon dioxide (200 nm), thermally grown on 500-550 µm thick <100> silicon served as substrates (non intentionally doped). The sample size was 1x1cm². Chitosan films were spin-coated at 3000 $r.min^{-1}$ with an acceleration of 300 $r.s^{-2}$ and during 70 s. Then, a soft bake was performed on a hot plate at 150 °C during 5 min. No adhesion promoter layer was required due to good adhesion properties of chitosan with silicon oxide thanks to hydrogen bonds[25]. This resulted in films with a good reproducibility in thickness of about 100 nm (115 ± 3 nm for Ch35 and 98 ± 1 nm for Ch1). Film thickness was measured by reflectometry with an Ocean Optics spectrometer and values were based on measurements on 3 samples. AZ5214E resist was diluted with its solvent (PGMEA) at 1:2 (v/v). Spin coating was proceeded at 5500 $r.min^{-1}$ during 30 s and a soft bake followed on a hot plate at 110 °C during 60 s to obtain a 119 ± 7 nm thick film. PMMA resist was spin coated at 4000 $r.min^{-1}$ during 30 s and soft baked at 180 °C during 90 s to obtain 190 ± 6 nm thick blanket films.

For Infrared analyses, chitosan films were obtained by spin-coating (1000 $tr.min^{-1}$, 4000 $tr.s^{-2}$ during 2 min) on a 100 µm thick double sided polished intrinsic silicon wafer. Soft bake was performed on a hot plate at 150 °C during 5 min.

For SEC analyses, thicker (few microns) self-supporting films on silica (200 nm on Si) were obtained by allowing the chitosan solution to dry directly on the substrates in a desiccator, under vacuum, at room temperature and protected from light for several days.

## *B. Plasma processing and characterization*

Chitosan films were etched by reactive ion etching plasma (RIE Corial 200S etch system, 13.56 MHz RF generator) using the recipes based on fluorinated gases developed to etch silica[1] (operating conditions are displayed in TABLE II). The substrate temperature was set to 20 °C during etching. These experimental conditions were chosen so that the plasma is assumed to be stable. A pre-conditioning of the etching chamber with the gas to be used was done during 4min. For the surface analysis study in section III.A, the etching time was arbitrarily chosen to keep at least half of the initial resin thickness. As the plasma etching with $SF_6$/Ar is faster, the time was 15 s instead of 2 min for $CHF_3$. For the in-depth modification study in section III.C, films were longer exposed to plasma (30 min) with a physical filter on top. Two filters were used: a $MgF_2$ filter that transmits wavelength greater than 120 nm (thus including (V)UV), and a glass filter coated with Indium Tin Oxide that transmits wavelength greater than 330 nm.

TABLE II. RIE plasma conditions applied to etch silica

| Gas | Gas flow (sccm) | Pressure (mT) | RF Power (W) | Bias voltage (V) | Silica etching rate ($nm.min^{-1}$) |
|---|---|---|---|---|---|
| $CHF_3$ | 100 | 50 | 140 | 580 | 54 |
| $SF_6$/Ar | 50/50 | 10 | 60 | 390 | 31 |

Plasma discharges were characterized by Optical Emission Spectroscopy end-point detection system EV-140C from Horiba. Spectrograph focal length was 140 mm and width slit was 100 µm. Detection was performed using CCD Line array detectors with 2048 pixels in a wavelength range of 200-800 nm.

## *C. Film characterization*

Water contact angle was performed with 1 µL of deionized ultrapure water using image capture (GBX Digidrop-MCAT). No repeatability could be performed because the first drop of water slightly dissolved the film.

Atomic Force Microscopy analysis was operated using a NX10 instrument from Park. Radius of curvature of the tip was less than 5nm. Image scan size was 5 µm x 5 µm with a resolution of 512 x 512 pixels. The surface roughness of the films was measured as the root mean square (RMS) of the surface height data.

X-ray photoelectron spectroscopy (XPS) analysis was performed using a VG Scienta SES 2002 spectrometer (Uppsala, Sweden) equipped with a monochromatic Al Kα X-ray source (Al Kα = 1486.6 eV) and a hemispherical analyzer, with pressure of $10^{-9}$ mbar in the analysis chamber. No electron gun was used to compensate the charging effect. The analyzed area was 24 $mm^2$. The spectra were recorded using a pass energy of 100 eV for high resolution and 500 eV for wide scan, respectively. Binding energies were calibrated by taking C1s peak (C-C, C-H) of carbon as a reference (285.0 eV). Analysis was done at an emission angle of 0° as measured from the surface normal. The peak fitting of the high-resolution spectra was performed using CasaXPS software version 2.3.14 and the peak

shape was Gaussian/Lorentzian (70/30). The background was subtracted using the Shirley method. Full width at half maximum (FWHM) was imposed equal for the different components of the same photoelectron peak within a sample, as far as possible. Double peak sulfur S2p was fitted[30] by fixing the binding energy difference between $2p_{1/2}$ and $2p_{3/2}$ at 1.18 eV, identical FWHM, and an area ratio of 0.45, thus a deviation of 0.05 from the theory (0.5).

ToF-SIMS measurements were carried out on a TRIFT III ToF-SIMS instrument (Physical Electronics, USA) operated with a pulsed 22 keV $Au^+$ ion gun (2nA ion current) rastered over a 300 × 300 $\mu m^2$ area. The electron gun was operated in pulsed mode at low electron energy for charge compensation. The ion dose was kept within the static conditions limit. Data were analyzed using the WinCadence software. Mass calibration was performed on hydrocarbon secondary ions. Mean values and standard deviations for some intensity ratios and normalized intensities were calculated from data obtained on three analysis areas. Normalization in the positive mode was performed on the total positive ion intensity from which were subtracted the intensity value of $H^+$ (due to possible changes as a function of very slight changes in the experimental settings) and that of $Na^+$. Normalization in the negative mode was performed on the total negative ion intensity from which was subtracted the intensity value of $H^-$(same reason as above).

Dissolution speed was calculated by immersing films in ultrapure water during 2 min. The films were then dried with a nitrogen spray blow gun and then on a hot plate at 150 °C during 1min. When the film dissolved completely, the immersion time was reduced to 30 s. The film thickness was measured before and after dissolution.

SEC analyses of chitosan films were performed as described above after dissolution of the films at 0.5 mg/mL in a 0.2 M acetic acid/0.15 M ammonium acetate buffer (pH 4.5) during a minimum of 24 h at ambient temperature. The solutions were then filtered using 0.45 µm pore size CME membranes (Millipore).

Transmission infrared measurements were carried out on a FTIR Vertex70V Bruker, with a DTGS detector, KBr/Ge beam splitter and under primary vacuum. Instrumental resolution was $4cm^{-1}$ and average was done on 64 scans at the nanocharacterization platform (PFNC) of CEA-Leti.

# III. RESULTS AND DISCUSSION

## *A. Chitosan behavior in contact with fluorinated etching plasmas*

### *1. Fluorinated plasma characterization*

$CHF_3$ and $SF_6$/Ar RIE etching plasmas (see plasma conditions in Table II) were first characterized using Optical Emission Spectroscopy (OES).

FIG. 1(a) and (b) show their optical emission spectra in the 200-800 nm range. As referred to the emission lines in FIG. 1(a), $SF_6$/Ar (50/50 sccm) mostly exhibits emissions related to atomic fluorine (680-720 nm) and to argon (Ar I lines at 750 nm and in the 350-400 nm range). As no $SF_x$ (x=1-6) radical species were significantly detected (a broad band with a peak at 289.3 nm should have then been observed[31,32]), the multi-step dissociation seems to be complete. However a really weak and broad band at 200-250 nm could be

related either to $SF_6$ dissociation species[33] or to $SO^-$ at 258 nm [34], which are probably due to interaction of sulfur species with the reactor walls. On the contrary, in pure $CHF_3$ plasma (FIG. 1(b)), only $CF_x$ radicals (200-300 nm) were detected and thus, no emission from atomic fluorine was evidenced.

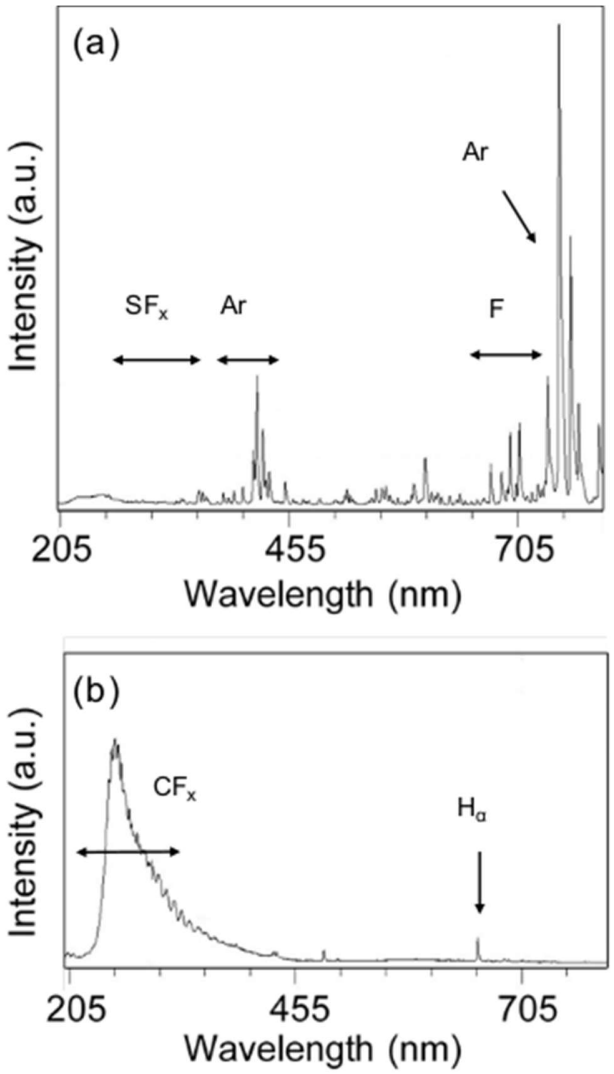


FIG. 1. Optical Emission Spectra (OES) of (a) $SF_6$/Ar plasma at 50/50 sccm, 10 mT, 60 W and (b) $CHF_3$ plasma at 100 sccm, 50 mT, 140 W, both in the RIE reactor

## *2. Resists etching behavior*

TABLE III displays chitosan resist etch rates and then selectivity values. The selectivity is here defined as the ratio between the etch rate of silica over that of the resist. Selectivity of Ch1 and Ch35 in $CHF_3$ plasma were 3.5 and 2.8, respectively. It was thus observed that Ch1 exhibited an etch resistance 1.25 higher than Ch35. In $SF_6$/Ar plasma, etch behavior was not the same as it can be expected from the OES analysis results. Ch1 and Ch35 were etched at 240 nm/min and 200 nm/min, respectively, which is about one order of magnitude faster than in $CHF_3$ plasma (20 nm/min etch rate for Ch35). Selectivity values for Ch1 and Ch35 in $SF_6$/Ar plasma were quite similar and relatively low (0.1 and 0.2, respectively).

Selectivity was also studied under the same conditions for conventional resists. In $CHF_3$ plasma, PMMA and novolac-based resist (AZ5214E) exhibited a selectivity of 1.3 and 9.0, respectively. It means that chitosan exhibits a better etching resistance than the conventional PMMA resist in $CHF_3$ plasma but lower than a novolac-based resist. However, in $SF_6$/Ar plasma, etch rates of conventional resists and chitosan are higher and selectivity are less than 1.

TABLE III. Selectivity, etch rates, Ohnishi Numbers (ON) and Ring Parameters (RP) for chitosan and conventional resists in $CHF_3$ and $SF_6$/Ar plasmas. "nr" refers to no ring in the chemical structure

| Resist name | $CHF_3$ | | $SF_6$/Ar | | ON | RP |
|---|---|---|---|---|---|---|
| | Selectivity | Etch rate ($nm.min^{-1}$) | Selectivity | Etch rate ($nm.min^{-1}$) | | |
| Ch1 | 3.5 | 16 ± 2 | 0.16 | 200 ± 9 | 11.0 | 0.4 |
| Ch35 | 2.8 | 20 ± 1 | 0.13 | 240 ± 5 | 10.3 | 0.4 |
| AZ5214E | 9.0 | 6 ± 0 | 0.70 | 44 ± 0 | 14 | 0.7 |
| PMMA | 1.3 | 43 ± 3 | 0.23 | 132 ± 3 | 5 | nr |

In order to compare resins in contact with etching plasmas, predictive parameters for etching have been developed empirically. The Ohnishi Number (ON)[35] predicts an increase of the etching rate when the ON increases. The Ring Parameter (RP)[36] indicates that when there is more carbon atoms in cycles (RP tends to 1), the etch resistance is higher. Their values were calculated and are also given in Table III. The trends announced by the ON do not fit with our observations and therefore it is not adapted to our case. More precisely, the oxygen content is similar for both chitosan samples, it seems then that this parameter is not sufficiently accurate in some cases as already pointed out in the literature[37]. The RP correctly anticipates the trends between the different resins, but exhibits limitations when the polymers are different but with the same number of cycles, as it is the case between chitosans with different DA. Therefore, surface and in-depth characterizations of chitosan in contact with fluorinated etching plasmas were undertaken in order to get a better understanding of the underlying mechanisms.

## *B. Surface analysis of chitosan in contact with fluorinated etching plasmas*

In plasma glow discharge, ions, radicals and neutrals can interact and then modify the resin at the surface within a few nanometers depth. In this section, various top surface analysis techniques (water contact angle, Atomic Force Microscopy, X-ray Photoelectron Spectroscopy and Time of Flight-Secondary Ion Mass Spectrometry) were used to gain information on changes in hydrophobicity, roughness and surface chemistry of Ch1 and Ch35 due to the interaction with fluorinated etching plasmas. Please note that as indicated in the experimental section, the exposure time was arbitrarily chosen to keep at least half of the initial resin thickness. As the plasma etching with $SF_6$/Ar is faster, the time was 15 s instead of 2 min for $CHF_3$. No quantitative comparison was then attempted, our goal being to give a qualitative comparison between the involved mechanisms in the specific case of the polysaccharide studied in our work (chitosan).

The water contact angles (WCA) of chitosan films are displayed in TABLE IV. It was observed that, for the pristine surfaces, when the DA increases, the water contact angle decreases. This has already been discussed in the literature[38,39]. The hydrophobic character is influenced by the acetyl group distribution along the chain[40]. Also, more acetyl groups help to create more hydrogen bonds with water. Furthermore, it is interesting to note that after contact with fluorinated etching plasmas, it seems that chitosan, regardless of the DA, exhibits the same surface hydrophobicity (around 90° for $CHF_3$ and 73° for $SF_6$/Ar). The higher WCA after $CHF_3$ plasma might indicate a different modification of the surface chemistry (graphitization or Teflon®-like deposition[41,42]) and/or roughness.

TABLE IV. Water contact angles for chitosan films (Ch1 and Ch35) and for chitosan films after 2 min in $CHF_3$ plasma and after 15 s in $SF_6$/Ar plasma (see experimental section for the justification)

| | Pristine film | Film after $CHF_3$ plasma | Film after $SF_6$/Ar plasma |
|---|---|---|---|

| | | | |
|---|---|---|---|
| Ch1 | 83° | 88° | 74° |
| Ch35 | 50° | 91° | 72° |

Plasma exposure could create roughness at the surface of the resist and it was studied using Atomic Force Microscopy (AFM). Images (5x5 $\mu m^2$) were acquired and Root Mean Square (RMS) values were calculated. The RMS values displayed were calculated from the average of 2 different areas on the same sample. FIG. 2 shows the Ch35 film before and after 2 min in $CHF_3$ and after 15 s in $SF_6$/Ar plasmas ((a), (b), (c) respectively). Images (1x1 $\mu m^2$) were also acquired with increased lateral resolution ((d), (e), (f), respectively). Pristine film is quite homogenous and exhibits a RMS value of 0.4 nm. After 2 min in $CHF_3$ plasma and after 15 s in $SF_6$/Ar plasma, RMS values were calculated as 2.3 nm and 1.6 nm, respectively. Regular granular aspect surfaces were observed in FIG. 2 (e) and (f). Qualitatively, after 2 min in $CHF_3$ plasma, grains appeared round and bigger than after $SF_6$/Ar plasma.

For the Ch1 film, AFM images – data not shown- were very similar to those obtained for the Ch35 film, exhibiting notably the same grain morphology. However, RMS values did exhibit some difference. Pristine Ch1 film, before, after 2 min in $CHF_3$ plasma and after 15 s in $SF_6$/Ar plasma, gave RMS values of 0.64 nm, 1.2 nm and 1.1 nm, respectively. We note that the pristine films (Ch1 and Ch35) exhibited rather similar RMS values.

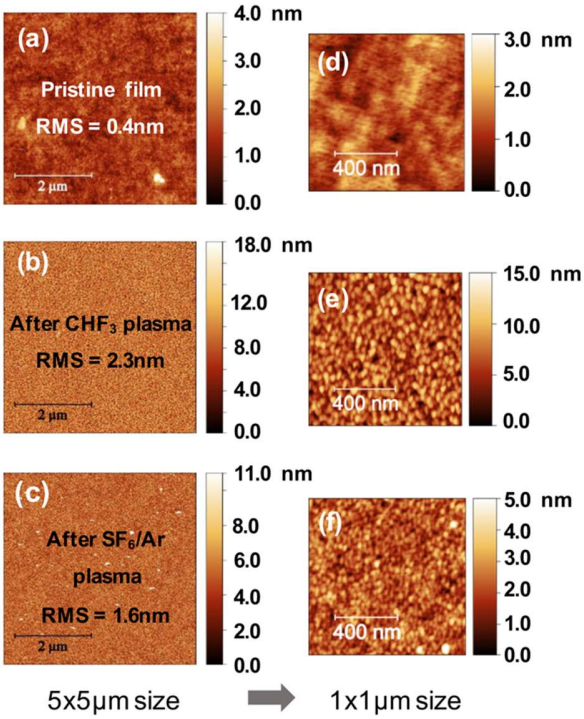


FIG. 2. 5x5µm images obtained using AFM of (a) a pristine chitosan Ch35 film, (b) Ch35 after 2 min in $CHF_3$ plasma and (c) Ch35 after 15 s in $SF_6$/Ar plasma. 1x1 µm images were acquired to better see grain differences in (d), (e) and (f), respectively. Please note that the Z-scales are different for the various images.

Roughness formation can be explained mainly by two phenomena[43] : the buckling model and the micro-masking. The buckling model is based on the concept of a thin dense layer on top of a thicker softer layer (which may have been modified by the plasma)[44,45], which induces stress relaxation and leads to wrinkle formation. No wrinkles have been observed and therefore this hypothesis is not favored. Micro-masking can also lead to roughness formation when non-volatile species produced during etching are deposited at the film surface[43].

In addition, some parameters have a key role in roughness formation and could be used to differentiate the observations between Ch1 and Ch35. The chemistry and the structure of the polymer play an important role[37]. For example, after interactions with the $C_4F_8$/90 % Ar plasma, the 193 nm methacrylate-based photoresist (MAMA/α-GBLMA) was observed to exhibit more roughness than the 248 nm polyhydroxystyrene-based resist which remained rather smooth[43]. Etching time could also play a role, because for two resists similar to those discussed above, the evolution of the surface roughness is different[46].

To conclude this AFM study, since grain morphologies are similar for Ch1 and Ch35 chitosan films after exposure to $CHF_3$ (2 min) or $SF_6$/Ar plasmas (15 s), but the RMS values are different, it is difficult to address the interplay between a physical etching of the chitosan layer and a (re)deposition process of different species. Indeed, the formation of roughness can be due to several sources. One may wonder if the amine or acetyl groups influence the potential plasma-surface interaction.

To get a better insight on the modification of chitosan film, the study of the surface chemical composition of the chitosan resists (Ch1 and Ch35) after exposure to etching plasmas was undertaken by XPS and ToF-SIMS. XPS atomic percentages were extracted from high resolution spectra and Ch35 results are displayed in TABLE V. The reasoning will be done with Ch35 that is why the results for Ch1 are not presented.

TABLE V. XPS atomic percentages at the surface of a pristine Ch35 chitosan film and Ch35 chitosan films after contact with fluorinated plasmas (after 2 min in $CHF_3$ plasma and after 15 s in $SF_6$/Ar plasma) (etching was stopped before the complete removal of the film - see experimental section for the justification)

| *C(% at)* | Pristine film | After $CHF_3$ plasma | After $SF_6$/Ar plasma |
|---|---|---|---|

| | | | |
|---|---|---|---|
| C1s | 58.8 | 58.0 | 57.8 |
| O1s | 33.4 | 8.7 | 28.5 |
| N1s | 7.8 | 3.1 | 7.2 |
| F1s | | 30.2 | 5.3 |
| S2p | | | 1.2 |

For the pristine Ch35 film, oxygen, carbon and nitrogen were detected as expected from the chitosan chemical structure. Oxygen/Nitrogen (O/N) and Carbon/Oxygen (C/O) ratios were calculated. The theoretical values correspond to 4.4 for O/N and to 1.5 for C/O. Calculated ratios from experimental values corresponded to 4.3 for O/N and 1.8 for C/O. They are thus consistent with the theoretical values with still a slightly higher C/O ratio. After 2 min in $CHF_3$ plasma, fluorine was detected (30.2 %), which is consistent with the increase in hydrophobicity of the exposed surface and the nature of the plasma gas. While there was a significant decrease in oxygen and nitrogen atomic percentages, carbon atomic percentage remained similar. After 15 s in $SF_6$/Ar plasma, even if fluorine was detected, its atomic percentage (5.3 %) was much lower than after 2 min in $CHF_3$ plasma. Low amount of sulfur was also detected (1.2 %).

FIG. 3 shows XPS C1s photoemission high resolution spectra of the Ch35 chitosan resist. See supplementary material at [URL will be inserted by AIP Publishing] for high resolution of O1s, N1s, F1s and S2p spectra (FIG. S1). Pristine film C1s spectra are displayed in FIG 3(a). Binding energy was calibrated by setting the C-C/C-H peak at 285.00 eV. Two other peaks at 286.4 eV and 287.9 eV were assigned to C-N/C-O and O-C-O/C=O, respectively. Oxygen O1s could be fitted with two contributions: O=C-N from

the acetyl group (531.4 eV) and OH-C/O-C-O from the hemiacetal and the hydroxyl groups (532.7 eV). Finally, nitrogen was detected as both N from amine ($NH_2$) and amide (N-C=O) at 399.4 eV. The peak at 401.4 eV was attributed to $NH_3^+$.

After 2 min in $CHF_3$ plasma (FIG. 3(b)), C1s was fitted with C-C/C-H and C-N/C-O peaks but also additional contributions which were attributed to fluorocarbon had to be included. C-F, C-$F_2$ and C-$F_3$ were detected at 288.4 eV, 290.6 eV and 293.0 eV, respectively. C-$CF_x$, was also included in the C-N/C-O peak at 286.1 eV because binding energies are similar (286.9 eV[47]). Moreover, the O-C-O/C=O peak was decreased consistently with the O atomic percentage. Fluorine was fitted by one simple peak at 687.8 eV that corresponded to F-C so the fluorine detected at the surface of the resist was only of fluorocarbon type. The number of carbon atoms in C-F bonds ($N_{C\text{-}F}$ = 2640) is somewhat similar to the number of fluorine atoms in F-C bonds ($N_{F\text{-}C}$ = 2623) In the literature, it has been reported that etching using fluorocarbon plasma leads to a competitive process between the etching of the resist and the deposition of a fluorocarbon layer on the silicon surface[48]. XPS results on chitosan after 2 min $CHF_3$ plasma are consistent with such a mechanism. Indeed, the decrease in the atomic percentages of chitosan elemental signatures (O and N) could be the result of not only the sputtering of the chitosan layer but also the detection of a fluorocarbon top layer (limiting the observation of chitosan due to the XPS information depth). Similar results were obtained after 2 min $CHF_3$ plasma for Ch1 (data not displayed). Moreover, similar C1s signatures on silicon and oxide silicon were found when they were exposed to $CHF_3$ plasma[47] and on photoresist surface exposed to $C_4F_8$/90 % Ar plasma[37].

After 15 s in $SF_6$/Ar plasma (FIG. 3(c)), chitosan surface did not exhibit similar features. The C1s signal was very similar to that of the pristine chitosan with only the additional contribution at 288.5 eV assigned to C-F. Fluorine F1s was fitted with one peak that corresponds to F-C at 688.1 eV. $N_{F\text{-}C}$ was calculated to be 13 % higher than $N_{C\text{-}F}$. Similar results were obtained for the Ch1 resist. When considering other atoms to which some fluorine atoms could be bond, no chemical shifts were in agreement with those found in the literature. Indeed, NaF would have given a peak around 683.5 eV[49]. Another hypothesis is that fluorine could be bound to silicon in SiF (F1s at 686.8 eV[50, 47]) or SiOF (687.4 eV[47]). In the survey spectrum, it is possible to observe a very small contribution from silicon but the peak was not well resolved. Alternatively, fluorine could be bond to sulfur, as in $SF_x$[51], but peaks should have been detected at 688.2 eV (F1s) and 173.5 eV (S2p2/3). It could fit for F1s but the S2p contribution at 173.5 eV was not observed. Therefore, sulfur chemical shift is not in favor of a bond with fluorine atom. As a summary for the chitosan films after 15 s in $SF_6$/Ar plasma, XPS spectra were very similar to those of the pristine chitosan with only small intensity additional signatures from fluorine and sulfur. No $C_xF_y$ layer could be evidenced as it was the case after the 2 min $CHF_3$ plasma. The C-F bonds can then be rather due to some grafting of fluorine atoms to the surface.

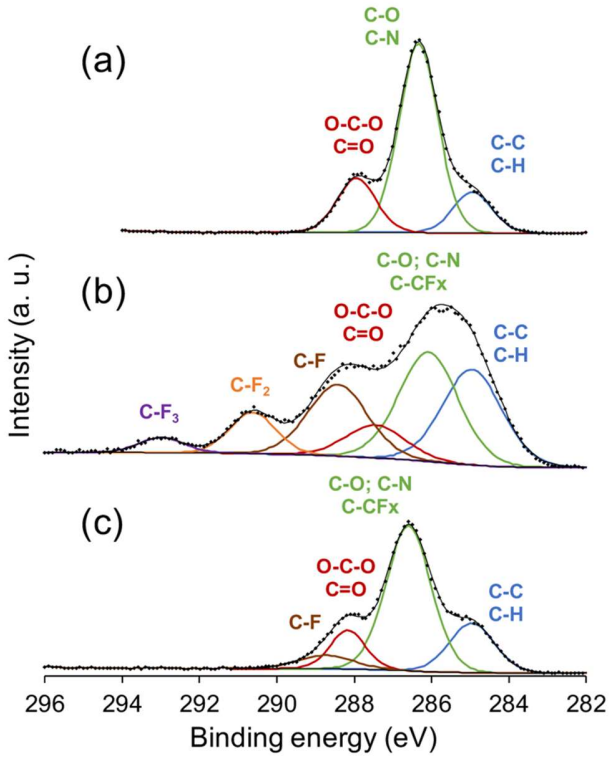


FIG. 3. High resolution XPS spectra of the C1s peak from the Ch35 chitosan resist (a) pristine film, (b) after 2 min in $CHF_3$ plasma and (c) after 15 s in $SF_6$/Ar plasma (etching was stopped before the complete removal of the film - see experimental section for the justification).

ToF-SIMS analysis was then performed to gain complementary information on the top surface molecular composition (information depth is limited to a few monolayers[52]). The positive mode spectra of the Ch35 chitosan film before and after contact with fluorinated etching plasmas (similar conditions as above) are displayed in FIG. 4.

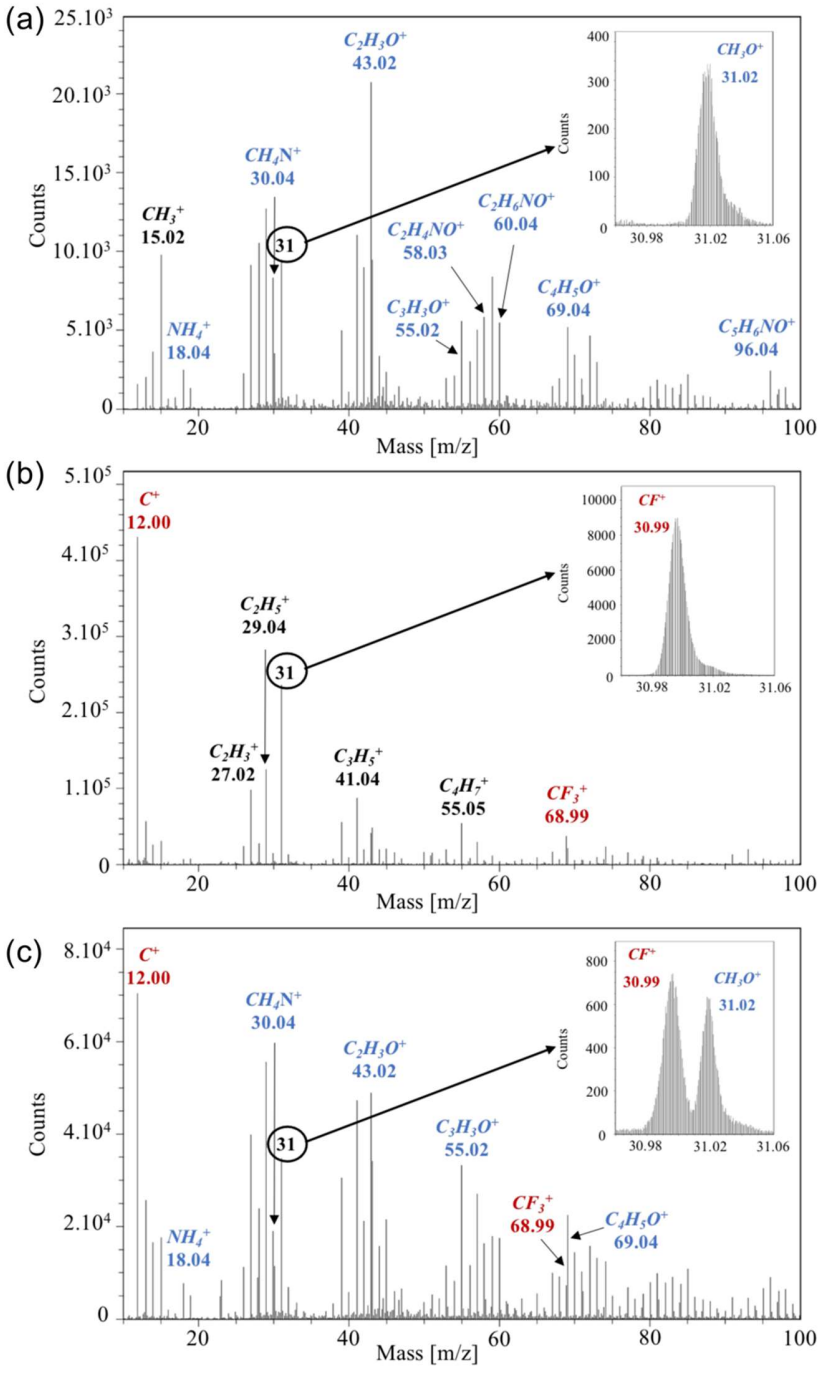


FIG. 4. ToF-SIMS positive mode spectra in the m/z = 10 to 100 range for (a) the pristine Ch35 chitosan film, (b) Ch35 after 2 min in $CHF_3$ plasma and (c) Ch35 after 15 s in $SF_6$/Ar plasma (etching was stopped before the complete removal of the film - see experimental section for the justification).

Chitosan characteristic signatures could be easily identified at the surface of the pristine film in the m/z range displayed in FIG. 4(a). Amine groups[53,54] can be followed by a.o. peaks at m/z = 18.04 ($NH_4^+$), 30.04 ($CH_4N^+$) in the positive mode spectra and at m/z = 26.00 ($CN^-$) in the negative mode spectra (data not displayed). Also, m/z = 31.02 ($CH_3O^+$), 42.00 ($CNO^-$) (data not displayed), 43.02 ($C_2H_3O^+$), 58.03 ($C_2H_4NO^+$) and 60.04 ($C_2H_6NO^+$) were assigned to chitosan characteristic signatures. No secondary ion of the complete chitosan monomer was detected but high mass molecular ions corresponding to backbone fragments[53] could be detected at m/z = 96.04 ($C_5H_6NO^+$) but also at higher m/z (not displayed in the figure) such as at m/z = 112.03 ($C_5H_6NO_2^+$), 126.06 ($C_6H_8NO_2^+$) and 144.07 ($C_6H_{10}NO_3^+$). At m/z = 59.04, 73.03 and 147.03, peaks can correspond to chitosan signatures[53] but also to signatures from a polydimethylsiloxane (PDMS) ubiquitous contamination[55]. They were then not included in the chitosan specific signatures. Please note also that ToF-SIMS being a highly sensitive technique[52], a very slight $F^-$ signature was also identified at the surface of the pristine film (before any contact with plasma).

After 2 min in $CHF_3$ plasma, negative mode spectrum was dominated by fluorine related signatures: m/z =18.99 ($F^-$), 37.99 ($F_2^-$) (data not displayed). In the positive mode spectrum (see FIG. 4(b)), peaks at m/z = 30.99 ($CF^+$), 68.99 ($CF_3^+$) were significantly detected. The $CF_2^+$ contribution was also detected but at a lower relative intensity. It was also possible to identify several other specific $C_xF_y^+$ signatures with higher x and y values such as peaks at m/z 85.99 ($C_4F_2^+$), 92.99 ($C_3F_3^+$), 99.98 ($C_2F_4^+$), 111.98 ($C_3F_4^+$), 118.99 ($C_2F_5^+$), 130.98 ($C_3F_5^+$), 140.98 ($C_7F_3^+$) but no intense signatures from the chitosan backbone grafted with fluorine could be observed. It was still possible to detect a few contributions combining oxygen and fluorine, such as $OF^-$ (34.99) or $C_3OF^+$ (70.99) but

they exhibited very low relative intensity. This limited contribution as well as the detection of numerous intense $C_xF_y^{+/-}$ contributions and the decrease in relative intensity of chitosan molecular signatures (see normalized intensities of secondary ions of interest in TABLE VI), indicate that these results did not specifically point to fluorine grafting to the chitosan backbone but are predominantly consistent with the deposition of a fluorocarbon top layer, which is fully consistent with the XPS results. Fluorocarbon signatures $C_xF_y^{+/-}$ with high x and y values are indeed typical to a fluorocarbon plasma deposited layer[56,57]. Plasma deposition is the predominant mechanism in $CHF_3$ plasma but the high sensitivity of ToF-SIMS also indicates that some grafting signatures might be detected to a very limited extent.

TABLE VI. Normalized intensity (NI) of ToF-SIMS secondary ions which are chitosan characteristic peaks for the pristine Ch35 film, Ch35 after 2 min in $CHF_3$ plasma and Ch35 after 15 s in $SF_6$/Ar plasma (etching was stopped before the complete removal of the film - see experimental section for the justification)

| Signatures | Pristine Ch35 film NI (x10000) | Ch35 after $CHF_3$ plasma NI (x10000) | Ch35 after $SF_6$/Ar plasma NI (x10000) |
|---|---|---|---|
| $NH_4^+$ | 69.4 ± 1.5 | 22.8 ± 1.0 | 42.9 ± 2.7 |
| $CH_4N^+$ | 321.8 ± 0.9 | 48.6 ± 1.1 | 155.8 ± 6.8 |
| $CN^-$ | 430.2 ± 5.1 | 64.0 ± 3.0 | 556.0 ± 9.1 |
| $CH_3O^+$ | 261.5 ± 3.3 | 68.6 ± 15.7 | 92.2 ± 5.2 |
| $C_2H_3O^+$ | 673.2 ± 14.6 | 151.2 ± 0.6 | 313.6 ± 14.0 |
| $C_2H_4NO^+$ | 164.8 ± 6.8 | 11.2 ± 0.5 | 75.5 ± 5.5 |
| $C_2H_6NO^+$ | 143.0 ± 7.0 | 4.9 ± 0.1 | 77.8 ± 5.2 |
| $CNO^-$ | 153.7 ± 3.1 | 5.2 ± 0.3 | 105.0 ±0.7 |
| $C_5H_6NO^+$ | 69.2 ± 2.8 | 16.3 ± 0.6 | 50.0 ± 2.1 |

| | | | |
|---|---|---|---|
| $C_5H_6NO_2^+$ | 25.7 ± 1.0 | 2.0 ± 0.1 | 22.4 ± 1.9 |
| $C_6H_8NO_2^+$ | 23.0 ± 1.9 | 1.5 ± 0.2 | 24.8 ± 0.4 |
| $C_6H_{10}NO_3^+$ | 25.5 ± 2.4 | 1.7 ± 0.1 | 15.7 ± 0.4 |

After 15 s in $SF_6$/Ar plasma, ToF-SIMS spectra (see positive mode spectrum in FIG. 4(c)) exhibited signatures of chitosan but also fluorine containing peaks including new peaks that could indicate a combination of fluorine with sulfur and with chitosan backbone. Chitosan signatures were characterized by lower relative intensities than for the pristine film but much higher than for the Ch35 film after 2 min in $CHF_3$ plasma (see TABLE VI). More precisely, fluorine was detected at m/z = 18.99 ($F^-$), 37.99 ($F_2^-$), in fluorocarbon signatures at m/z 30.99 ($CF^+$), 68.99 ($CF_3^+$) but also in secondary ions that might combine chitosan fragments with fluorine atoms (for example at m/z = 66.01 that could correspond to $CH_2NF_2^-$ or $CH_3O_2F^-$) and on the other hand that might combine fluorine with sulfur at m/z = 50.97 ($SF^-$) but no $SF_x^-$ ion was identified. No $C_xF_y^+$ contributions with high x and y values were detected, except a very low relative intensity for $C_3F_3^+$. Sulfur was detected at m/z 31.97 ($S^-$ but not completely separated from $O_2^-$), as well as with low relative intensity $SO^-$ (47.98) and $SO_2^-$ (63.97). Also, it was possible to detect carbon-sulfur bond at m/z = 44.98 ($CHS^+$). Silicon was detected alone (m/z 27.97) and at low relative intensity combined with fluorine at m/z = 46.97 ($SiF^+$). ToF-SIMS results are thus again consistent with XPS, showing more signatures indicating grafting and less signatures showing a layer deposition. For Ch1, normalized intensity signature $C_2H_3O^+$ was not decreasing after plasma, but all other signatures followed the trend observed for Ch35. In summary, after 15 s in $SF_6$/Ar plasma, Ch35 and Ch1 are not displaying any fluorocarbon film deposition and the few detected fluorocarbon signatures

were rather attributed to some grafting as also evidenced by signatures combining fluorine with other elements.

The overall summary is then that Ch35 and Ch1 after 2 min in fluorocarbon plasma are mostly characterized by a mechanism involving deposition of a $C_xF_y$ layer (XPS and ToF-SIMS). This layer provides protection against a fast etching and improve then the etching resistance[45,58]. This behavior makes chitosan resist suitable for silica etching with $CHF_3$ independently of the DA. On the contrary, after 15 s in $SF_6$/Ar plasma, no deposition layer was observed. Fluorine atoms were detected but grafted on the top surface of the etched resist. This indicates a major physical interaction between atomic species of the plasma and the chitosan surface.

## C. *In-depth analysis of chitosan film in contact with fluorocarbon plasma*

During plasma etching, ion/neutrals and radicals can interact with surface sample, but it is also the case for the UV emitted by the plasma. While the ions interact with the top surface, the UV interacts more deeply. UV and VUV can break bonds thanks to their energy. Photons that have sufficient energy to break most of all polymer bonds, are photons with $\lambda$<250 nm[59]. Therefore, chitosan exposed to VUV light could undergo in-depth chemical changes. To observe these possible changes, chitosan films were exposed to $SF_6$/Ar and $CHF_3$ plasmas while being protected by a longpass filter on top of the surface. $MgF_2$ filter has a cut off at 120 nm while the glass filter with an ITO layer on top has a cut off at 330 nm. In this last case, we can consider that the chitosan film is almost not exposed to the UV/VUV of the plasma whereas with the $MgF_2$ filter, it was considered to be exposed. The reference was a pristine film.

Regarding the selectivity and surface analyses, we have focused our UV/VUV plasma interaction interest on Chitosan films exposed to $CHF_3$ plasma. The emission in UV/VUV was applied to the films during 30 min and were characterized using their dissolution speed in deionized (DI) water, Size-Exclusion Chromatography and Infrared Spectroscopy.

Data on the dissolution speed of chitosan films in deionized water during 2 min are displayed in TABLE VII. For the samples exposed to UV>120 nm, the films were completely dissolved within less than 2 min and dissolution time was reduced to 30 s. as it was a good tradeoff between time measurement accuracy and film dissolution state.

TABLE VII. Dissolution speed (in $nm.min^{-1}$) in DI water for pristine (not exposed) films and for films after UV exposure from a $CHF_3$ plasma. The slash symbol refers to impossible calculation due to the complete removal of the film left after time limit (30 s). $\lambda$ >120 nm refers to $MgF_2$ filter ((V)UV are included) and $\lambda$>330 nm refers to glass/ITO filter used (no/limited (V)UV).

| Resist name | Pristine film | $\lambda$ >120 nm (including (V)UV) | $\lambda$ >330 nm (no/limited (V)UV) |
|---|---|---|---|
| Ch1 | 2.5 ± 0.4 | / | 5.0 ± 1.0 |
| Ch35 | 6.5 ± 0.4 | / | 4.2 ± 0.5 |

The dissolution speed of chitosan pristine films was 2.5 $nm.min^{-1}$ for Ch1 and 6.5 $nm.min^{-1}$ for Ch35. After exposure to light with $\lambda$>330 nm (no/limited (V)UV), dissolution film was slightly modified. Note the slight difference between the two DA. Ch35 dissolved slightly slower after exposure to $\lambda$> 330 nm while Ch1 dissolved a bit faster. However, after exposure of the chitosan film to light with $\lambda$ >120 nm ((V)UV are included), the resist was totally soluble in DI water, even during a shorter time (30 s). These changes in solubility suggest that probably the resist undergoes structural modifications. As reported by several authors, the increased solubility may be the results of chain scissions [60,61,62].

Therefore, Mw variation before and after UV exposure was evaluated using SEC and results are displayed in FIG. 5.

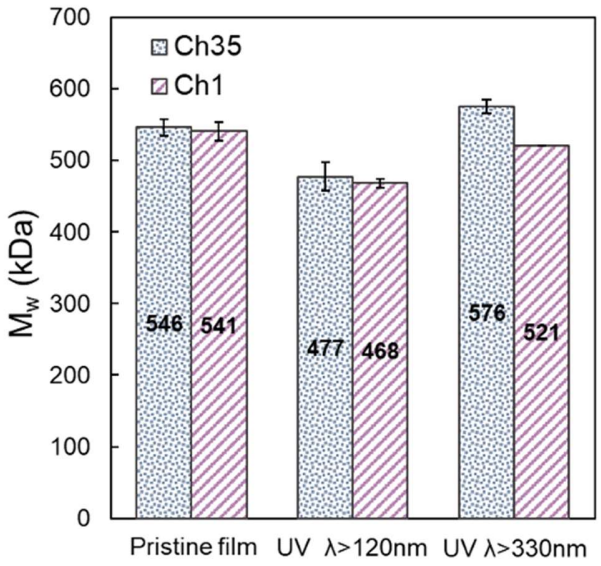


FIG. 5. Average weight molar mass (Mw) variation measured by size-exclusion chromatography of pristine chitosan film (not exposed) and $CHF_3$ UV plasma exposed chitosan films. $\lambda$ >120 nm refers to $MgF_2$ filter ((V)UV are included) and $\lambda$>330 nm refers to glass/ITO filter used (no/limited (V)UV).

Pristine film of chitosan has a Mw around 540-550 kDa for both DA. After being exposed to $CHF_3$ plasma $\lambda$> 330nm (no/limited (V)UV), Ch35 and Ch1 Mw increased by 30 kDa and decreased by 20 kDa, respectively. It may be interesting to note that the slight difference observed is logical with respect to that observed with the dissolution rates. For Ch35, increase of the Mw after contact with $CHF_3$ plasma $\lambda$>330 nm (no/limited (V)UV) may be due to either cross-linking or SEC measurement uncertainty. A small trend is emerging when comparing to the dissolution speed results. On the one hand, Ch35 Mw was observed to slightly increase after $\lambda$>330 nm (no/limited (V)UV) irradiation and on the other hand, the dissolution speed slightly decreases. The same logic can be applied to Ch1 resist where the slight decrease in Mw coincides with a higher dissolution speed.

However, the main differences appear for samples exposed to $\lambda$ >120 nm ((V)UV are included). The drop in Mw was nearly 70 kDa. This has already been observed in the literature when chitosan was exposed to UV but the experimental conditions were different[60,61]. Sionkowska *et al*[60] found that viscosity average molecular weight of chitosan films decreased when exposed to light under 254 nm emitted from a UV lamp for 2 h to 24 h. This weight molar mass loss was explained by chain scissions under UV (formation of free radicals). Wasikiewicz *et al*[61] also observed a decrease in weight molar mass of chitosan solution when exposed to a UV lamp (wavelength range not given) but during shorter times (up to 15 min). In all cases, the molecular weight loss was two orders of magnitude. In our case, the Mw loss was lower and the reason for this may come from the partial insolation of the film. UV penetration depth is highly linked to its wavelength and to the resist. For example, UV in the range [200-380 nm] can penetrate a few microns within polymer films[63]. In the case of a 193 nm methacrylate based photoresist, VUV<200 nm can penetrate up to 100-200 nm while in the case of a 248 nm photoresist, it is around 15-40 nm penetration depth[63]. Chitosan films of about 150 nm could be supposed to be completely or almost irradiated (IR spectroscopy analysis). But those of several microns in thickness as one used for SEC analysis are assumed to be fully exposed of UV and partially to VUV (thin thickness exposed). The film is therefore not modified uniformly but in layers or gradient[63].

To conclude, a small but non-negligible decrease in Mw was observed after $CHF_3$ plasma $\lambda$ >120 nm ((V)UV are included) irradiation. This suggests a chain scission phenomenon, which would lead to lower Mw, whatever the difference in DA. However due to the penetration depth of the light, this was limited to the first 10-100 nm of the film.

The FTIR spectrum of the pristine chitosan Ch35 film without any plasma exposure is displayed in FIG. 6. The main peaks corresponding to chitosan can be found in the literature. The broad absorption band at 3355 $cm^{-1}$ corresponds to both O-H and N-H stretchings[64,65,66]. The absorption band at 2866 $cm^{-1}$ can be attributed to C-H stretching[64,67], the one at 1660 $cm^{-1}$ corresponds to C=O stretching in amide I group[40,66,68] and the one at 1545 $cm^{-1}$ is attributed to N-H bending[66,67,69]. The sharp band between 900 and 1150 $cm^{-1}$ corresponds to C-O stretching of chitosan[64,68], with C-O-C from skeletal at 1080 $cm^{-1}$ and 1135 $cm^{-1}$ for C-O-C from glucosidic unit bridge[64, 66,69].

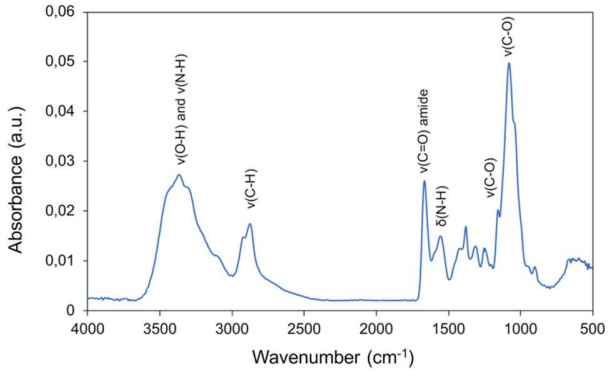


FIG. 6. FTIR spectrum of the pristine chitosan (Ch35) film

To observe plasma UV effects on the resist, films were exposed to $CHF_3$ plasma during 30 min with a longpass filter (either $MgF_2$ filter or ITO/glass filter) on top. FTIR spectrum of the pristine film and of the films exposed to different ranges of UV are displayed in FIG. 7 (a). The dotted line shows the difference between a reference film and the film that was exposed to the plasma with the $MgF_2$ filter ($\lambda$ >120 nm ((V)UV are included)). Four modifications can be observed in the spectrum and presented in FIG. 7 (b) to (e). Loss of signal intensity was observed in the range between 3000 and 3700 $cm^{-1}$ with

a maximum at 2870 $cm^{-1}$ that corresponds to both O-H stretching and N-H stretching. The decrease in OH and NH signature absorption can indicate O-H and N-H bond scissions. However, because of the overlapping of the peaks it is difficult to conclude on this decrease in intensity. Another decrease was observed at 2870 $cm^{-1}$ and 2920 $cm^{-1}$. It corresponds to the range of C-H stretching. Another decrease corresponds to the C-O bonds in the C-O-C group at 1037 $cm^{-1}$ and 1076 $cm^{-1}$ and could reflect ring opening of GlcN units and/or chain scission at glycosidic bonds. On the FIG. 7 (d), the difference between pristine film and film exposed to $CHF_3$ plasma $\lambda$ >120 nm ((V)UV are included) is plotted to better visualize the maximum wavelength differences. Changes that appear on FIG. 7 (a) are visible in FIG. 7 (d) at 1725 $cm^{-1}$. Absorbance gains were observed at 1630 $cm^{-1}$, 1697 $cm^{-1}$and 1725 $cm^{-1}$ that correspond to C=O bonds in different chemical groups.

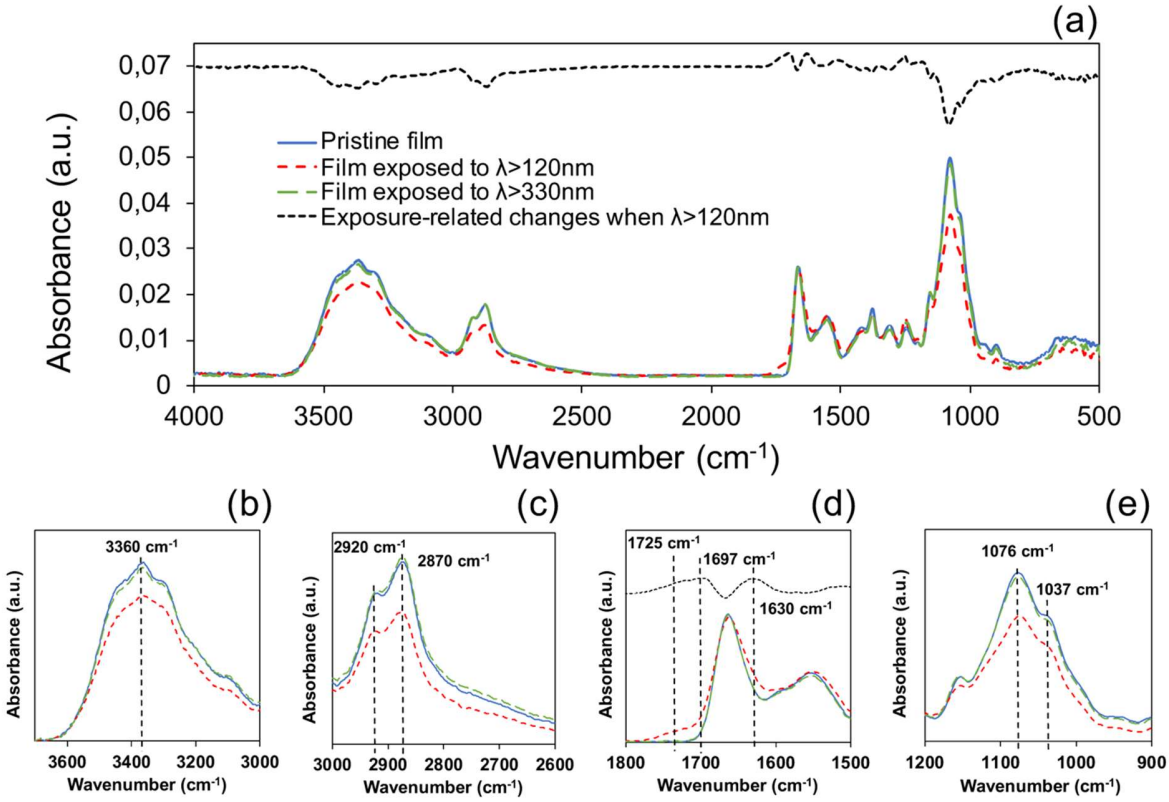


FIG. 7. FTIR spectra of the Ch35 pristine film and of the $CHF_3$ UV-exposed Ch35 films. (a) General spectra and specific ranges where infrared signal was different. (b) 3000-3700 $cm^{-1}$, (c) 2600-3000 $cm^{-1}$, (d) 1500-1800 $cm^{-1}$ and (e) 900-1200 $cm^{-1}$. $\lambda$ >120 nm refers to $MgF_2$ filter ((V)UV are included) and $\lambda$>330 nm refers to glass/ITO filter used (no/limited (V)UV).

To summarize, under $\lambda$ >120 nm ((V)UV are included) from the $CHF_3$ plasma, chitosan degradation can be characterized by the loss of C-O-C functions and the creation of C=O bonds. This can correspond to an opening of the unit ring and/or the scission of glycosidic bonds and the formation of carbonyl functions. This is in agreement with what has been observed on chitosan under other conditions[70,71,72]. Also, it was seen that the loss of C-O-C functions was accompanied by a peak appearance at 1730 $cm^{-1}$, that corresponds

to the accumulation of oxidation products[72]. This peak was also observed in our spectra as it was explained above and could suggest that under our conditions chitosan degradation also forms oxidation products.

Similarly, the spectra of the Ch1 films were acquired. See supplementary material at [URL will be inserted by AIP Publishing] for Ch1 FTIR spectrum before and after UV exposure (FIG. S2 and S3, respectively). The spectrum of the pristine film is as expected slightly different because there is almost no amide in the chitosan Ch1 but the amine peak comes out at 1604 $cm^{-1}$. Under UV from the $CHF_3$ plasma, the trends observed for the Ch1 resist are similar to those observed for Ch35. No/very little modifications were observed when using the ITO/glass filter. Whereas with $\lambda$ >120 nm ((V)UV are included) ($MgF_2$ filter), there was a difference in absorption intensities similar to those described for Ch35: a decrease in absorbance for C-O-C groups, C-H groups, but almost no change for O-H/N-H group. Also, an increase at 1650 $cm^{-1}$ (C=O) and 1555 $cm^{-1}$ that corresponds to amide[73] and finally the appearance of a shoulder at 1749 $cm^{-1}$, which as indicated above, could correspond to oxidation products.

Bussière *et al*[72] proposed a photooxidation mechanism of chitosan degradation, presented in FIG. 8, under accelerated conditions ($\lambda$>300 nm, at 60° and in presence of $O_2$). Under irradiation, there is abstraction of a hydrogen from the chitosan and thus formation of a radical. Depending on the position of the carbon to which the hydrogen was bound, the mechanism is different. This can lead to either a separation of the acetyl groups (carbon a), to a scission of the glycosidic bonds (carbon b) or to a ring opening that forms an amide group (carbon c). It also indicates an IR band specific to each mechanism such as the appearance of a band at 1730 $cm^{-1}$ which might be related to the degradation mechanism

by scission of glycosidic bonds. The changes in IR bands in comparison with the proposed mechanism, suggests that there could be 2 possible chitosan degradations. First, degradation by scission of glycosidic bonds, related to the apparition of band at 1730 $cm^{-1}$ and ring opening (gain of carbonyl bonds at 1697 $cm^{-1}$). The relative proportion of these mechanisms could not be clearly identified.

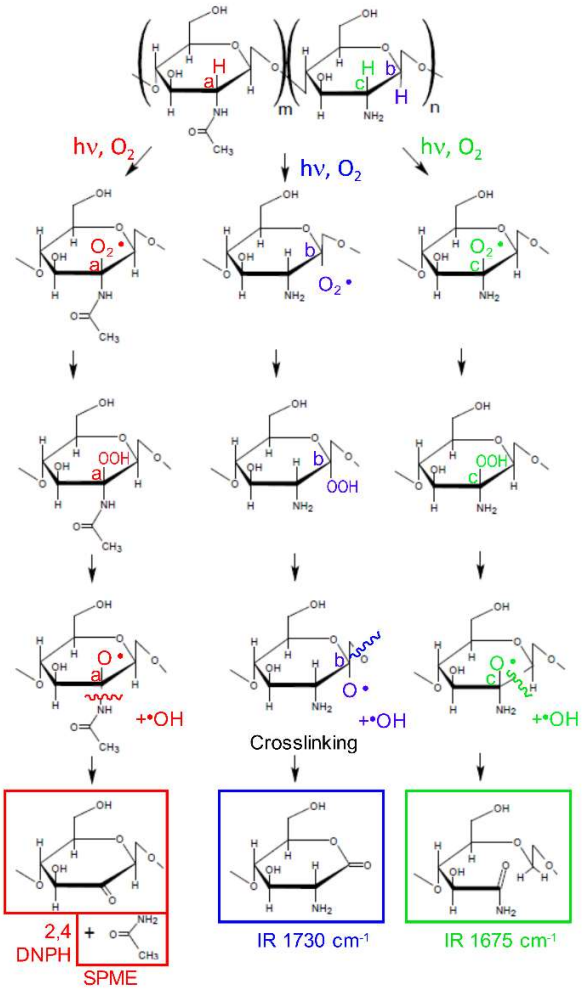


FIG. 8. Chitosan photo-oxidation mechanism proposed by Bussière *et al*[72]. Reprinted from P. Bussiere, J. Gardette, G. Rapp, C. Masson, and S. Therias, Carbohydr. Polym. 259,117715 (2021) with permission from Elsevier.

Chitosan degradation was attributed to free radicals[61] notably the hydroxyl one[74,60] which is known to be really active. Chitosan degradation under DUV can be similar to the one under gamma radiation[61]. Hydroxyl radical may come from chitosan itself by abstraction of a hydrogen atom[72] or from homolysis of the water contained in the film. Water is absorbing strongly in the VUV range[75,76,77] and forms hydroxyl radicals, that can interact with chitosan and therefore there will be a degradation of the resist according to the mechanisms described above.

In a review, Popovic *et al*[78] collected the emissions of $CHF_3$ gases at low-pressure plasma. Fluorocarbon $CF_2$ components can emit in the VUV range (136.2-159.0 nm), atomic fluorine emits light with wavelength under 100 nm, and carbon atom emission stands between 100 and 200 nm. In the work of Woodworth et al (in the same review), C lines, F lines and CF lines (198; 203; 208; 214 nm) were detected in capacitive coupling plasma ICP. Some carbon C* and $CF_2$* radical lines from 110 to 190 nm were also detected for plasma in a CCP reactor by Popovic *et al*[78]. It is possible to hypothesize that the $CHF_3$ plasma in our conditions (CCP), also emits in the VUV wavelengths <200 nm. So based on this hypothesis, water is potentially absorbing during $CHF_3$ plasma. Chitosan is absorbing around 200 nm[26]. VUV has enough energy to break chitosan bonds, so it can create molecular radicals by chain scissions, which can thus trigger the chain reaction.

To summarize, under $CHF_3$ specific UV plasma exposition, chitosan resist undergoes modifications. The degradation mechanism could be related to oxygen reactive radical creation, that can come from the absorption of radiation by water contained in the film or the scission of bonds of chitosan. This may lead to chain reaction by scission of glycosidic bonds and/or ring opening. This can explain a decrease in molar mass and a

greater solubility in water. These last changes are relatively small, notably because of the partial insolation of the thick films prepared for SEC analysis. Nevertheless, they are significant enough to be considered.

# IV. SUMMARY AND CONCLUSIONS

Chitosan has been demonstrated to be a possible candidate to be used as a resist in lithography processes. In the present study, the interaction of chitosans with $SF_6$/Ar and $CHF_3$ etching plasmas was studied. Two chitosan resists with similar Mw but different degrees of acetylation were compared. Surface analytical tools, chromatography and infra-red spectroscopy were used to address these modifications at the surface of the chitosan films as well as more in depth.

Our results show that the selectivity of chitosan in $CHF_3$ plasma arises from the deposition of a fluorocarbon film and that the selectivity is not significantly different for the two chitosans. Furthermore, under $SF_6$/Ar plasma, there was no evidence of a similar fluorocarbon film deposition, which limited the selectivity. Our results also suggest that VUV emitted by the plasma are responsible for chain scissions at the glycosidic bonds and/or ring opening, leading to a decrease in Mw. However, only extensive exposure time (30 minutes) lead to in depth measurable modifications. Therefore, the selectivity is probably merely affected by VUV radiations with less than 2 minutes etching time.

The good selectivity of chitosan films compared to silica when using $CHF_3$ plasma, should allow for the transfer of features into 200 nm silica hardmask and will be the focus of future studies.

## ACKNOWLEDGMENTS

ANR Lithogreen, ANR-19-CE43-0009, is acknowledged for financial support and Nanolyon for technical support. NMR spectra were performed at CCRMN (Centre Commun de RMN de Lyon 1).

## AUTHOR DECLARATIONS

The authors have no conflicts to disclose

## DATA AVAILABILITY

The data that support the findings of this study are available within the article and supplementary material.

# REFERENCES


[1] J.W. Coburn, “Plasma-Assisted Etching,” Plasma Chem. Plasma Process. **2**(1), 1–41 (1982).

[2] C.F. Chelton, M. Glowatz, and J.A. Mosovsky, “Chemical hazards in the semiconductor industry,” IEEE Trans. Educ. **34**(3), 269–288 (1991).

[3] M. Jang, C. Yoon, J. Park, and O. Kwon, “Evaluation of hazardous chemicals with material safety data sheet and by-products of a photoresist used in the semiconductor-manufacturing industry,” Saf. Health Work **10**(1), 114–121 (2019).

[4] B. Jiang, J. Yang, C. Li, L. Zhang, X. Zhang, and P. Yang, “Water-Based Photo- and Electron-Beam Lithography Using Egg White as a Resist,” Adv. Mater. Interfaces **4**(7), 1601223 (2017).

[5] R.K. Pal, and V.K. Yadavalli, “Silk protein nanowires patterned using electron beam lithography,” Nanotechnology **29**(33), 335301 (2018).

[6] J. Park, S.G. Lee, B. Marelli, M. Lee, T. Kim, H.K. Oh, H. Jeon, F.G. Omenetto, and S. Kim, “Eco-friendly photolithography using water-developable pure silk fibroin,” RSC Adv. **6**(45), 39330–39334 (2016).

[7] S. Kim, B. Marelli, M.A. Brenckle, A.N. Mitropoulos, E.S. Gil, K. Tsioris, H. Tao, D.L. Kaplan, and F.G. Omenetto, “All-water-based electron-beam lithography using silk as a resist,” Nat. Nanotechnol. **9**(4), 306–310 (2014).

[8] J. Morikawa, M. Ryu, K. Maximova, A. Balčytis, G. Seniutinas, L. Fan, V. Mizeikis, J. Li, X. Wang, M. Zamengo, X. Wang, and S. Juodkazis, “Silk fibroin as a water-soluble bio-resist and its thermal properties,” RSC Adv. **6**(14), 11863–11869 (2016).

[9] S. Zhang, N. Qin, and T.H. Tao, “Extracted natural silk fibroin as a dual-tone protein resist for eco-friendly electron beam lithography,” IEEE Int. Conf. Micro Electro

Mech. Syst., 724–727 (2017).

[10] A. Bucciarelli, R.K. Pal, D. Maniglio, A. Quaranta, V. Mulloni, A. Motta, and V.K. Yadavalli, "Fabrication of Nanoscale Patternable Films of Silk Fibroin Using Benign Solvents," Macromol. Mater. Eng. **302**(7), 1700110 (2017).

[11] Z. Liu, Z. Zhou, H. Tao, and K. Liu, "Direct patterning using protein-based water lithography," IEEE Micro Electro Mech. Syst., 504–506 (2018).

[12] N.E. Kurland, T. Dey, S.C. Kundu, and V.K. Yadavalli, "Precise patterning of silk microstructures using photolithography," Adv. Mater. **25**(43), 6207–6212 (2013).

[13] W. Zeng, D. Yu, Y. Tang, C. Lin, S. Zhu, Y. Huang, Y. Lin, X.Y. Liu, and C. Wu, "Wool Keratin Photolithography as an Eco-Friendly Route to Fabricate Protein Microarchitectures," ACS Appl. Bio Mater. **3**(5), 2891–2896 (2020).

[14] W. Liu, Z. Zhou, S. Zhang, Z. Shi, J. Tabarini, W. Lee, Y. Zhang, S.N. Gilbert Corder, X. Li, F. Dong, L. Cheng, M. Liu, D.L. Kaplan, F.G. Omenetto, G. Zhang, Y. Mao, and T.H. Tao, "Precise Protein Photolithography (P3): High Performance Biopatterning Using Silk Fibroin Light Chain as the Resist," Adv. Sci. **4**(9), 1700191 (2017).

[15] K. Morita, K. Yamamoto, M. Harumoto, Y. Tanaka, C. Mori, Y. Arisawa, T. Motono, H. Stokes, and M. Asai, "High sensitivity non-CAR resists for EUV and EB lithography," Proc. SPIE, Adv. Patterning Mater. Process. XXXVII **11326**, 113260C (2020).

[16] S. Takei, A. Oshima, T. Ichikawa, A. Sekiguchi, M. Kashiwakura, T. Kozawa, S. Tagawa, T.G. Oyama, S. Ito, and H. Miyasaka, "Organic solvent-free water-developable sugar resist material derived from biomass in green lithography," Microelectron. Eng. **122**, 70–76 (2014).

[17] J.J. Zou, C.J. Liu, and B. Eliasson, "Modification of starch by glow discharge plasma," Carbohydr. Polym. **55**(1), 23–26 (2004).

[18] Y.C. Wu, T.M. Lee, J.C. Lin, S.Y. Shaw, and C.Y. Yang, "Argon-plasma-treated chitosan: Surface characterization and initial attachment of osteoblasts," J. Biomater. Sci. Polym. Ed. **21**(5), 563–579 (2010).

[19] D.C. Bastos, A.E.F. Santos, M.L.V.J. da Silva, and R.A. Simão, "Hydrophobic corn starch thermoplastic films produced by plasma treatment," Ultramicroscopy **109**(8), 1089–1093 (2009).

[20] P. Rachtanapun, D. Boonyawan, R.A. Auras, and G. Kasi, "Effect of Water-Resistant Properties of Kraft Paper ( KP ) Using sulfur hexafluoride ($SF_6$) plasma coating," Polymers (Basel). **14**, 3796 (2022).

[21] S. Voznesenskiy, A. Nepomnyaschiy, and Y. Kulchin, "Study of biopolymer chitosan as resist for submicron electronic lithography," Solid State Phenom. **213**, 180–185 (2014).

[22] S. Voznesenskiy, and A. Nepomnyaschiy, "Dose characteristics of multilayer chitosan-metal-dielectric nanostructures for electronic nanolithography," Solid State Phenom. **245**, 195–199 (2016).

[23] J.M. Karp, Y. Yeo, W. Geng, C. Cannizarro, K. Yan, D.S. Kohane, G. Vunjak-Novakovic, R.S. Langer, and M. Radisic, "A photolithographic method to create cellular micropatterns," Biomaterials **27**(27), 4755–4764 (2006).

[24] A.K. Grebenko, K.A. Motoviloc, A. V. Bubis, and A.G. Nasibulin, "Gentle patterning approaches toward compatibility with bio-organic materials and their environmental aspects," Small **18**(22), 2200476 (2022).

[25] M. Caillau, P. Crémillieu, E. Laurenceau, Y. Chevolot, J.-L. Leclercq, S. Alekseev, C. Chevalier, and T. Delair, "Fifty nanometer lines patterned into silica using water developable chitosan bioresist and electron beam lithography," J. Vac. Sci. Technol. B **35**(6), 06GE01 (2017).

[26] M. Caillau, C. Chevalier, P. Crémillieu, T. Delair, O. Soppera, B. Leuschel, C. Ray, C. Moulin, C. Jonin, E. Benichou, P. Brevet, C. Yeromonahos, E. Laurenceau, Y. Chevolot, and J.-L. Leclercq, "Sub-micron lines patterning into silica using water developable chitosan bioresist films for eco-friendly positive tone e-beam and UV lithography," Proc. SPIE, Opt. Microlithogr. XXXI **10587**, 105870S (2018).

[27] O. Sysova, P. Durin, C. Gablin, D. Léonard, A. Teolis, T. Delair, D. Berling, I. Servin, R. Tiron, A. Bazin, J.-L. Leclercq, Y. Chevolot, and O. Soppera, "Chitosan as

water developable 193 nm photoresist for green photolithography," ACS Appl. Polym. Mater. **4**(6), 4508–4519 (2022).

[28] G. Lamarque, J.M. Lucas, C. Viton, and A. Domard, "Physicochemical behavior of homogeneous series of acetylated chitosans in aqueous solution: Role of various structural parameters," Biomacromolecules **6**(1), 131–142 (2005).

[29] C. Schatz, C. Viton, T. Delair, C. Pichot, and A. Domard, "Typical Physicochemical Behaviors of Chitosan in Aqueous Solution," Biomacromolecules **4**(3), 641–648 (2003).

[30] G. Beamson, and D. Briggs, *High Resolution XPS of Organic Polymers : The Scienta Esca300 Database* (John Wiley & Sons Ltd, Chichester, 1992).

[31] Z.L. Petrovic, F. Tochikubo, S. Kakuta, and T. Makabe, "Spatiotemporal optical emission spectroscopy of rf discharges in $SF_6$," J. Appl. Phys. **73**(5), 2163 (1993).

[32] H.M. Anderson, J.A. Merson, and R.W. Light, "A Kinetic Model for Plasma Etching Silicon in a $SF_6/O_2$ RF Discharge," IEEE Trans. Plasma Sci. **14**(2), 156–164 (1986).

[33] K.H. Shim, Y.H. Kil, H.D. Yang, B.K. Park, J.H. Yang, S. Kang, T.S. Jeong, and T.S. Kim, "Characteristics of germanium dry etching using inductively coupled $SF_6$ plasma," Mater. Sci. Semicond. Process. **15**(4), 364–370 (2012).

[34] X. Li, H. Zhou, C.D.W. Wilkinson, and I.G. Thayne, "Optical Emission Spectrometry of Plasma in Low-Damage Sub-100 nm Tungsten Gate Reactive Ion Etching Process for Compound Semiconductor Transistors," Jpn. J. Appl. Phys. **45**(10B), 8364–8369 (2006).

[35] H. Gokan, S. Esho, and Y. Ohnishi, "Dry Etch Resistance of Organic Materials," J. Electrochem. Soc. **130**(1), 143–146 (1983).

[36] R.R. Kunz, S.C. Palmateer, A.R. Forte, R.D. Allen, G.M. Wallraff, R.A. DiPietro, and D.C. Hofer, "Limits to etch resistance for 193-nm single-layer resists," Proc. SPIE, Adv. Resist Technol. Process. XIII **2724**, 365–376 (1996).

[37] S. Engelmann, R.L. Bruce, T. Kwon, R. Phaneuf, G.S. Oehrlein, Y.C. Bae, C. Andes,

D. Graves, D. Nest, E.A. Hudson, P. Lazzeri, E. Iacob, and M. Anderle, “Plasma-surface interactions of model polymers for advanced photoresists using $C_4F_8$/Ar discharges and energetic ion beams,” J. Vac. Sci. Technol. B **25**(4), 1353–1364 (2007).

[38] M. Gatto, D. Ochi, C.M.P. Yoshida, and C.F. da Silva, “Study of chitosan with different degrees of acetylation as cardboard paper coating,” Carbohydr. Polym. **210**, 56–63 (2019).

[39] L.J.R. Foster, S. Ho, J. Hook, M. Basuki, and H. Marçal, “Chitosan as a Biomaterial : Influence of Degree of Deacetylation on Its Physiochemical , Material and Biological Properties,” PLoS One **10**(8), e0135153 (2015).

[40] M. Rinaudo, “Chitin and chitosan : Properties and applications,” Prog. Polym. Sci. **31**(7), 603–632 (2006).

[41] W.A. Daoud, J.H. Xin, Y.H. Zhang, and C.L. Mak, “Pulsed laser deposition of superhydrophobic thin Teflon films on cellulosic fibers,” Thin Solid Films **515**(2), 835–837 (2005).

[42] S. Vaswani, J. Koskinen, and D.W. Hess, “Surface modification of paper and cellulose by plasma-assisted deposition of fluorocarbon films,” Surf. Coat. Technol. **195**(2–3), 121–129 (2005).

[43] G.S. Oehrlein, R.J. Phaneuf, and D.B. Graves, “Plasma-polymer interactions: A review of progress in understanding polymer resist mask durability during plasma etching for nanoscale fabrication,” J. Vac. Sci. Technol. B **29**(1), 010801 (2011).

[44] R.L. Bruce, F. Weilnboeck, T. Lin, R.J. Phaneuf, G.S. Oehrlein, B.K. Long, C.G. Willson, J.J. Vegh, D. Nest, and D.B. Graves, “Relationship between nanoscale roughness and ion-damaged layer in argon plasma exposed polystyrene films,” J. Appl. Phys. **107**(8), 084310 (2010).

[45] A. Pranda, S.A. Gutierrez Razo, Z. Tomova, J.T. Fourkas, and G.S. Oehrlein, “Role of the dense amorphous carbon layer in photoresist etching,” J. Vac. Sci. Technol. A **36**(2), 021304 (2018).

[46] X. Hua, S. Engelmann, G.S. Oehrlein, P. Jiang, P. Lazzeri, E. Iacob, and M. Anderle,

"Studies of plasma surface interactions during short time plasma etching of 193 and 248 nm photoresist materials," J. Vac. Sci. Technol. B Microelectron. Nanom. Struct. **24**(4), 1850–1858 (2006).

[47] C. Cardinaud, A. Rhounna, G. Turban, and B. Grolleau, "Analyse XPS des surfaces de Si et $SiO_2$ exposées aux plasmas de $CHF_3$ et $CHF_3$—$C_2F_6$. Polymérisation et gravure," Rev. Phys. Appliquée **24**(3), 309–321 (1989).

[48] F. Garboriau, M.C. Fernandez-Peignon, G. Cartry, and C. Cardinaud, "Etching mechanisms of Si and $SiO_2$ in inductively coupled fluorocarbon plasmas : Correlation between plasma species and surface etching," J. Vac. Sci. Technol. A **23**(2), 226–233 (2005).

[49] Y. Kawamoto, K. Ogura, M. Shojiya, M. Takahashi, and K. Kadono, "F 1s XPS of fluoride glasses and related fluoride crystals," J. Fluor. Chem. **96**(2), 135–139 (1999).

[50] P.Y. Tessier, T. Chevolleau, C. Cardinaud, and B. Grolleau, "An XPS study of the $SF_6$ reactive ion beam etching of silicon at low temperatures," Nucl. Instruments Methods Phys. Res. B **155**(3), 280–288 (1999).

[51] G.B. Fisher, N.E. Erikson, E. Madey, and J.T. Yates, "X-ray photoemission study of physically absorbed $SF_6$," Surfaces Sci. **65**(1), 210–228 (1977).

[52] A. Benninghoven, "Chemical Analysis of Inorganic and Organic Surfaces and Thin Films by Static Time-of-Flight Secondary Ion Mass Spectrometry (ToF-SIMS)," Angew. Chemie Int. Ed. **33**(10), 1023–1043 (1994).

[53] L. Tortora, S. Concolato, M. Urbini, S.M. Giannitelli, F. Basoli, A. Rainer, M. Trombetta, M. Orsini, and P. Mozetic, "Functionalization of poly (ε-caprolactone) surface with lactose-modified chitosan via alkaline hydrolysis : ToF-SIMS characterization," Biointerphases **11**(2), 02A323 (2016).

[54] B. Lepoittevin, T. Elzein, D. Dragoe, A. Bejjani, F. Lemée, J. Levillain, P. Bazin, P. Roger, and I. Dez, "Hydrophobization of chitosan films by surface grafting with fluorinated polymer brushes," Carbohydr. Polym. **205**(1), 437–446 (2019).

[55] R.N.S. Sodhi, "Time-of-flight secondary ions mass spectrometry (ToF-SIMS) :

versatility in chemical and imaging surface analysis," Analyst **129**, 483–487 (2004).

[56] P. Lazzeri, X. Hua, G.S. Oehrlein, E. Iacob, M. Barozzi, M. Bersani, and M. Anderle, "ToF-SIMS and AFM studies of low-k dielectric etching in fluorocarbon plasmas," Appl. Surf. Sci. **252**(19), 7186–7189 (2006).

[57] F. Lewis, S. Turgeon, P. Chevallier, J. Pireaux, M. Tatoulian, and D. Mantovani, "On the Growth of Fluorocarbon Thin Films Deposited on Plasma-Etched 316L Stainless Steel," Plasma Process. Polym. **7**(3–4), 309–317 (2010).

[58] A. Pranda, S.A. Gutierrez Razo, J.T. Fourkas, and G.S. Oehrlein, "Evolution of photoresist layer structure and surface morphology under fluorocarbon-based plasma exposure," Plasma Process. Polym. **16**(9), 1900026 (2019).

[59] J.F. Rabek, *Photodegradation of Polymer : Physical Characteristics and Applications* (Springer, Berlin, Heidelberg, 1996).

[60] A. Sionkowska, A. Płanecka, K. Lewandowska, B. Kaczmarek, and P. Szarszewska, "Influence of UV-irradiation on molecular weight of chitosan," Prog. Chem. Appl. Chitin Its Deriv. **18**, 21–28 (2013).

[61] J.M. Wasikiewicz, F. Yoshii, N. Nagasawa, R.A. Wach, and H. Mitomo, "Degradation of chitosan and sodium alginate by gamma radiation , sonochemical and ultraviolet methods," Radiat. Phys. Chem. **73**(5), 287–295 (2005).

[62] I. Zainol, H.M. Akil, and A. Mastor, "Effect of γ-irradiation on the physical and mechanical properties of chitosan powder," Mater. Sci. Eng. C **29**(1), 292–297 (2009).

[63] F. Weilnboeck, R.L. Bruce, S. Engelmann, G.S. Oehrlein, D. Nest, T.-Y. Chung, D. Graves, M. Li, D. Wang, C. Andes, and E.A. Hudson, "Photoresist modifications by plasma vacuum ultraviolet radiation: The role of polymer structure and plasma chemistry," J. Vac. Sci. Technol. B **28**(5), 993–1004 (2010).

[64] M.R. Kasaai, "A review of several reported procedures to determine the degree of N -acetylation for chitin and chitosan using infrared spectroscopy," Carbohydr. Polym. **71**(4), 497–508 (2008).

[65] J. Brugnerotto, J. Lizardi, F.M. Goycoolea, W. Argüelles-Monal, J. Desbrières, and M. Rinaudo, "An infrared investigation in relation with chitin and chitosan characterization," Polymer (Guildf). **42**(8), 359–3580 (2001).

[66] N. Gholami, B. Jaleh, R. Golbedaghi, M.M. Larijani, P. Wanichapichart, M. Nasrollahzadeh, and R.. Varma, "Modification of Chitosan Membranes via Methane Ion beam," Molecules **25**(10), 2292 (2020).

[67] N. Mohamed, and N.G. Madian, "Evaluation of the mechanical , physical and antimicrobial properties of chitosan thin films doped with greenly synthesized silver nanoparticles," Mater. Today Commun. **25**, 101372 (2020).

[68] I. Corazzari, R. Nistico, F. Turci, M.G. Faga, F. Franzoso, S. Tabasso, and G. Magnacca, "Advanced physico-chemical characterization of chitosan by means of TGA coupled on-line with FTIR and GCMS : Thermal degradation and water adsorption capacity," Polym. Degrad. Stab. **112**, 1–9 (2015).

[69] G. Lawrie, I. Keen, B. Drew, A. Chandler-Temple, L. Rintoul, P. Fredericks, and L. Grøndahl, "Interactions between Alginate and Chitosan Biopolymers Characterized Using FTIR and XPS," Biomacromolecules **8**(8), 2533–2541 (2007).

[70] A. Sionkowska, H. Kaczmarek, M. Wisniewski, J. Skopinska, S. Lazare, and V. Tokarev, "The influence of UV irradiation on the surface of chitosan films," Surf. Sci. **600**(18), 3775–3779 (2006).

[71] U. Gryczka, D. Dondi, A.G. Chmielewski, W. Migdal, A. Buttafava, and A. Faucitano, "The mechanism of chitosan degradation by gamma and e-beam irradiation," Radiat. Phys. Chem. **78**(7–8), 543–548 (2009).

[72] P. Bussiere, J. Gardette, G. Rapp, C. Masson, and S. Therias, "New insights into the mechanism of photodegradation of chitosan," Carbohydr. Polym. **259**, 117715 (2021).

[73] I.K.D. Dimzon, and T.P. Knepper, "Degree of deacetylation of chitosan by infrared spectroscopy and partial least squares," Int. J. Biol. Macromol. **72**, 939–945 (2015).

[74] S. Wang, Q. Huang, and Q. Wang, “Study on the synergetic degradation of chitosan with ultraviolet light and hydrogen peroxide,” Carbohydr. Res. **340**(6), 1143–1147 (2005).

[75] K. Zoschke, H. Bornick, and E. Worch, “Vacuum-UV radiation at 185 nm in water treatment - A review,” Water Res. **52**, 131–145 (2014).

[76] S. Gligorovski, R. Strekowski, S. Barbati, and D. Vione, “Environmental Implications of Hydroxyl Radicals ( • OH ),” Chem. Rev. **115**(24), 13051–13092 (2015).

[77] G. Gonzalez, E. Oliveros, W. Michael, and A.. Braun, “Vacuum-ultraviolet photolysis of aqueous reaction systems,” J. Photochem. Photobiol. **5**(3), 225–246 (2004).

[78] D. Popovic, M. Mozetic, A. Vesel, G. Primc, and R. Zaplotnik, “Review on vacuum ultraviolet generation in low-pressure plasmas,” Plasma Process. Polym. **18**(9), 2100061 (2021).

# TABLES

TABLE I. Chitosan based resists used in this study

| Resist name | DA (%) | Concentration % (w/v) | Mw ($kg.mol^{-1}$) | Water content (%) |
|---|---|---|---|---|
| Ch1 | 1 | 0.7 | 583 | 8.9 |
| Ch35 | 35 | 0.7 | 613 | 13.5 |

TABLE II. RIE plasma conditions applied to etch silica

| Gas | Gas flow (sccm) | Pressure (mT) | RF Power (W) | Bias voltage (V) | Silica etching rate ($nm.min^{-1}$) |
|---|---|---|---|---|---|
| $CHF_3$ | 100 | 50 | 140 | 580 | 54 |
| $SF_6$/Ar | 50/50 | 10 | 60 | 390 | 31 |

TABLE III. Selectivity, etch rates, Ohnishi Numbers (ON) and Ring Parameters (RP) for chitosan and conventional resists in $CHF_3$ and $SF_6$/Ar plasmas. “nr” refers to no ring in the chemical structure

| Resist name | $CHF_3$ | | $SF_6$/Ar | | ON | RP |
|---|---|---|---|---|---|---|
| | Selectivity | Etch rate ($nm.min^{-1}$) | Selectivity | Etch rate ($nm.min^{-1}$) | | |
| Ch1 | 3.5 | 16 ± 2 | 0.16 | 200 ± 9 | 11.0 | 0.4 |
| Ch35 | 2.8 | 20 ± 1 | 0.13 | 240 ± 5 | 10.3 | 0.4 |
| AZ5214E | 9.0 | 6 ± 0 | 0.70 | 44 ± 0 | 14 | 0.7 |
| PMMA | 1.3 | 43 ± 3 | 0.23 | 132 ± 3 | 5 | nr |

TABLE IV. Water contact angles for chitosan films (Ch1 and Ch35) and for chitosan films after 2 min in $CHF_3$ plasma and after 15 s in $SF_6$/Ar plasma (see experimental section for the justification)

| | Pristine film | Film after $CHF_3$ plasma | Film after $SF_6$/Ar plasma |
|---|---|---|---|
| Ch1 | 83° | 88° | 74° |
| Ch35 | 50° | 91° | 72° |

TABLE V. XPS atomic percentages at the surface of a pristine Ch35 chitosan film and Ch35 chitosan films after contact with fluorinated plasmas (after 2 min in $CHF_3$ plasma and after 15 s in $SF_6$/Ar plasma) (etching was stopped before the complete removal of the film - see experimental section for the justification)

| *C(% at)* | Pristine film | After $CHF_3$ plasma | After $SF_6$/Ar plasma |
|---|---|---|---|
| C1s | 58.8 | 58.0 | 57.8 |
| O1s | 33.4 | 8.7 | 28.5 |
| N1s | 7.8 | 3.1 | 7.2 |
| F1s | | 30.2 | 5.3 |
| S2p | | | 1.2 |

TABLE VI. Normalized intensity (NI) of ToF-SIMS secondary ions which are chitosan characteristic peaks for the pristine Ch35 film, Ch35 after 2 min in $CHF_3$ plasma and Ch35 after 15 s in $SF_6$/Ar plasma (etching was stopped before the complete removal of the film - see experimental section for the justification)

| Signatures | Pristine Ch35 film NI (x10000) | Ch35 after $CHF_3$ plasma NI (x10000) | Ch35 after $SF_6$/Ar plasma NI (x10000) |
|---|---|---|---|
| $NH_4^+$ | 69.4 ± 1.5 | 22.8 ± 1.0 | 42.9 ± 2.7 |
| $CH_4N^+$ | 321.8 ± 0.9 | 48.6 ± 1.1 | 155.8 ± 6.8 |
| $CN^-$ | 430.2 ± 5.1 | 64.0 ± 3.0 | 556.0 ± 9.1 |
| $CH_3O^+$ | 261.5 ± 3.3 | 68.6 ± 15.7 | 92.2 ± 5.2 |
| $C_2H_3O^+$ | 673.2 ± 14.6 | 151.2 ± 0.6 | 313.6 ± 14.0 |

| | | | |
|---|---|---|---|
| $C_2H_4NO^+$ | 164.8 ± 6.8 | 11.2 ± 0.5 | 75.5 ± 5.5 |
| $C_2H_6NO^+$ | 143.0 ± 7.0 | 4.9 ± 0.1 | 77.8 ± 5.2 |
| $CNO^-$ | 153.7 ± 3.1 | 5.2 ± 0.3 | 105.0 ±0.7 |
| $C_5H_6NO^+$ | 69.2 ± 2.8 | 16.3 ± 0.6 | 50.0 ± 2.1 |

TABLE VII. Dissolution speed (in $nm.min^{-1}$) in DI water for pristine (not exposed) films and for films after UV exposure from a $CHF_3$ plasma. The slash symbol refers to impossible calculation due to the complete removal of the film left after time limit (30 s). $\lambda$ >120 nm refers to $MgF_2$ filter ((V)UV are included) and $\lambda$>330 nm refers to glass/ITO filter used (no/limited (V)UV).

| Resist name | Pristine film | $\lambda$ >120 nm (including (V)UV) | $\lambda$ >330 nm (no/limited (V)UV) |
|---|---|---|---|
| Ch1 | 2.5 ± 0.4 | / | 5.0 ± 1.0 |
| Ch35 | 6.5 ± 0.4 | / | 4.2 ± 0.5 |

# FIGURE CAPTIONS

FIG. 1. Optical Emission Spectra (OES) of (a) $SF_6$/Ar plasma at 50/50 sccm, 10 mT, 60 W and (b) $CHF_3$ plasma at 100 sccm, 50 mT, 140 W, both in the RIE reactor

FIG. 2. 5x5µm images obtained using AFM of (a) a pristine chitosan Ch35 film, (b) Ch35 after 2 min in $CHF_3$ plasma and (c) Ch35 after 15 s in $SF_6$/Ar plasma. 1x1 µm images were acquired to better see grain differences in (d), (e) and (f), respectively. Please note that the Z-scales are different for the various images.

FIG. 3. High resolution XPS spectra of the C1s peak from the Ch35 chitosan resist (a) pristine film, (b) after 2 min in $CHF_3$ plasma and (c) after 15 s in $SF_6$/Ar plasma (etching was stopped before the complete removal of the film - see experimental section for the justification).

FIG. 4. ToF-SIMS positive mode spectra in the m/z = 10 to 100 range for (a) the pristine Ch35 chitosan film, (b) Ch35 after 2 min in $CHF_3$ plasma and (c) Ch35 after 15 s in $SF_6$/Ar plasma (etching was stopped before the complete removal of the film - see experimental section for the justification)

FIG. 5. Average weight molar mass (Mw) variation measured by size-exclusion chromatography of pristine chitosan film (not exposed) and $CHF_3$ UV plasma exposed chitosan films. $\lambda$ >120 nm refers to $MgF_2$ filter ((V)UV are included) and $\lambda$>330 nm refers to glass/ITO filter used (no/limited (V)UV).

FIG. 6. FTIR spectrum of the pristine chitosan (Ch35) film

FIG. 7. FTIR spectra of the Ch35 pristine film and of the $CHF_3$ UV-exposed Ch35 films. (a) General spectra and specific ranges where infrared signal was different. (b) 3000-3700 $cm^{-1}$, (c) 2600-3000 $cm^{-1}$, (d) 1500-1800 $cm^{-1}$ and (e) 900-1200 $cm^{-1}$. $\lambda$ >120 nm refers to $MgF_2$ filter ((V)UV are included) and $\lambda$>330 nm refers to glass/ITO filter used (no/limited (V)UV).

FIG. 8. Chitosan photo-oxidation mechanism proposed by Bussière *et al*[72]. Reprinted from P. Bussiere, J. Gardette, G. Rapp, C. Masson, and S. Therias, Carbohydr. Polym. 259, 117715 (2021) with permission from Elsevier.